

EFFECTS OF DENSITY CONTRASTS ON THE  
ORIENTATION OF STRESSES IN THE LITHOSPHERE:  
RELATION TO PRINCIPAL STRESS DIRECTIONS IN  
THE TRANSVERSE RANGES, CALIFORNIA

Leslie J. Sonder

Department of Earth Sciences, Dartmouth College,  
Hanover, New Hampshire

*Abstract.* The influence of stresses arising from horizontal density contrasts on the orientation and relative magnitudes of principal stresses in an otherwise uniform lithospheric stress field is investigated. A simple model is constructed, in which a local deviatoric stress due to a density anomaly, embedded within or just below the lithosphere, and a regionally constant deviatoric stress field are each approximated by biaxial tensors. The net stress field is obtained from the sum of the two. Both the relative magnitudes of principal stresses and the magnitude of the angular difference in principal stress direction of the summed tensor compared with that obtained in the absence of buoyancy forces depend on two parameters. The first is the ratio  $\tau/\tau'$ , where  $\tau$  is a measure of the magnitude of the regional deviatoric stress and  $\tau'$  is the magnitude of the stress arising from buoyancy forces associated with the density anomaly. The second parameter is the angle between the trend of the density anomaly and the direction of maximum compressional stress that obtains in the absence of any perturbation by the local buoyancy forces. The directions of the principal axes of the total stress field are found to differ by up to  $90^\circ$  from those of the reference stress field. The model is applied to the Transverse Ranges, California, where the observed  $23^\circ$  difference in orientation of principal horizontal compressive stress compared with the principal compressive stress direction in central California constrains the predicted value of  $\tau/\tau'$  to be approximately  $-0.4$ . This is consistent with an independently calculated range of  $\tau/\tau'$  in which  $\tau'$  is inferred from seismological constraints on the magnitude of density variations underneath the Transverse Ranges and  $\tau$  is inferred from observations of heat flow along the San Andreas

fault in central California. The agreement between the two estimates of  $\tau/\tau'$  supports the hypothesis that the observed differences in horizontal principal stress orientation in California can be explained by the combined influence of a local negative buoyancy force under the Transverse Ranges and a regional stress field associated with transcurrent deformation within the Pacific-North American plate boundary zone. The observed counterclockwise angular difference in principal horizontal stress direction in the Transverse Ranges compared with central California implies that the plane of maximum right lateral shear stress is also rotated counterclockwise relative to that in central California. This supports the possibility that the "big bend" in the San Andreas fault may be a consequence of the negative buoyancy forces acting in the Transverse Ranges, and not the cause of Transverse Ranges formation, as has often been assumed.

## 1. INTRODUCTION

It is well known that density contrasts within the lithosphere can lead to horizontal differences in the magnitude of lithospheric stress [e.g., Bott and Dean, 1972; Artyushkov 1973; Fleitout and Froidevaux, 1982]. It should also be evident that the buoyancy forces due to these density contrasts may also affect the orientation of the principal stresses, yet comparatively little notice has been taken of this. In this paper I develop a simple model to examine the effects of a density anomaly on the state of stress in the lithosphere, with particular attention paid to changes in the orientation of the principal stresses. The model is tested by comparison with observations from the Transverse Ranges, California, where there is good seismic evidence for a wedge-shaped region of anomalously high density in the upper mantle [Humphreys et al., 1984] and where there are significant differences in the orientation of the stress field compared with surrounding regions [e.g., Zoback et al., 1987].

Copyright 1990  
by the American Geophysical Union.

Paper number 90TC00369.  
0278-7407/90/90TC-00369\$10.00

## 2. METHOD

Although there are many factors that may affect the state of stress in the lithosphere, such as driving and resisting forces at the edges of plates, or differences in the strength of the lithosphere, the subject of interest here is variations in the stress field arising from horizontal density contrasts. Hence, for simplicity, the state of stress is approximated as that resulting from the linear superposition of two states of stress. The first, taken as a reference state, is assumed to include all other sources of stress except density variations near or at the base of the lithosphere, which are described by the second stress state. Since the purpose of this paper is to examine the extent to which buoyancy forces alone can modify the orientation of the principal stresses, the reference state is taken to be horizontally and vertically constant; it may be thus described by a single tensor with constant components. Although these assumptions represent an over-simplification, the simple model that can be derived from them provides useful insights into the effects of buoyancy forces on the orientation of stresses within the lithosphere.

I make the further assumption that the reference stress state  $\mathbf{T}$  is biaxial, with one principal axis vertical, and represents one of either compressional, tensional, or strike-slip states of stress:

Compression:

$$\mathbf{T} = \begin{bmatrix} -\tau & 0 & 0 \\ 0 & 0 & 0 \\ 0 & 0 & \tau \end{bmatrix} \quad (1a)$$

Tension:

$$\mathbf{T} = \begin{bmatrix} 0 & 0 & 0 \\ 0 & \tau & 0 \\ 0 & 0 & -\tau \end{bmatrix} \quad (1b)$$

Strike-slip:

$$\mathbf{T} = \begin{bmatrix} -\tau & 0 & 0 \\ 0 & \tau & 0 \\ 0 & 0 & 0 \end{bmatrix} \quad (1c)$$

All stresses are deviatoric, tensional stresses have positive sign, and  $\tau$  is always positive. The coordinate frame is shown in Figure 1; the  $z$  axis is vertical and the  $x$  axis is taken to be parallel to the direction of maximum horizontal compression. (Note that in the extensional case, the  $x$ -axis is parallel to the intermediate principal stress direction, since the maximum compressional stress is vertical.)

The deviatoric stress field arising from a local density anomaly depends on the shape and magnitude of the anomaly. Defining an  $x'$ - $y'$ - $z$  coordinate system so that  $z$  is vertical and  $x'$  and  $y'$  are parallel and perpendicular, respectively, to the long horizontal axis of the anomaly, I consider here a density anomaly of constant magnitude  $\Delta\rho$  and thickness  $L$  and whose extent in the  $x'$  direction is much greater than its width  $2w$ , so that variations in density in the  $x'$  direction can be neglected.

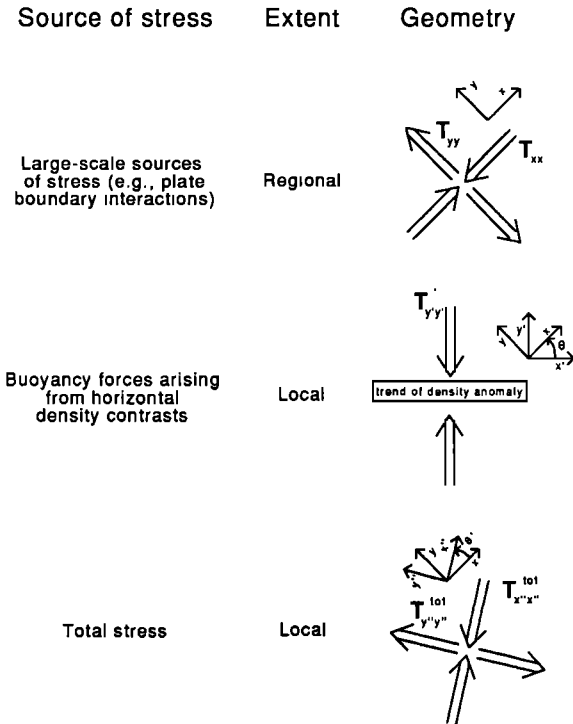


Fig. 1. Schematic description of model presented in section 2, showing orientation of regional stress tensor ( $\mathbf{T}$ ), stress tensor due to density anomaly ( $\mathbf{T}'$ ), and total stress tensor ( $\mathbf{T}^{\text{tot}}$ ), and definition of  $\theta$ ,  $\theta'$ , and coordinate systems. Double arrows indicate directions of principal horizontal components of  $\mathbf{T}$ ,  $\mathbf{T}'$ , and  $\mathbf{T}^{\text{tot}}$ .

Appendix A shows that, for the region above the density anomaly, the near-surface deviatoric stress field is approximately constant and may be expressed as a biaxial tensor in the ( $x'$ - $y'$ - $z$ ) coordinate system:

$$\mathbf{T}' = \begin{bmatrix} 0 & 0 & 0 \\ 0 & \tau' & 0 \\ 0 & 0 & -\tau' \end{bmatrix} \quad (2)$$

$\tau'$ , the magnitude of the components, is approximately  $0.3 \Delta\rho g - 0.4 \Delta\rho g$ , where  $g$  is the acceleration due to gravity. If  $\tau'$  is negative, this tensor represents a negative buoyancy force which would lead to a state of horizontal compression perpendicular to the trend of the anomaly; conversely, if  $\tau'$  is positive, horizontal tension is implied.

The coordinate frame ( $x'$ - $y'$ - $z$ ) in which  $\mathbf{T}'$  is defined does not generally coincide with the ( $x$ - $y$ - $z$ ) frame in which  $\mathbf{T}$  is defined. As shown in Figure 1, to express  $\mathbf{T}'$  in the same coordinate frame as  $\mathbf{T}$ ,  $\mathbf{T}'$  must be rotated through an angle  $\theta$  about a vertical axis. Thus,  $\theta$  is the angle between the trend of the density anomaly (the  $x'$ -axis) and the  $x$ -axis.

The net stress tensor,  $\mathbf{T}^{\text{tot}}$ , is the tensor sum of  $\mathbf{T}$  and  $\mathbf{T}'$  (Equations 1 and 2), and in the  $x$ - $y$ - $z$  reference frame may be written as:

Compression:

$$\mathbf{T}^{\text{tot}} = \begin{bmatrix} -\tau + \tau' \sin^2 \theta & \tau' \sin \theta \cos \theta & 0 \\ \tau' \sin \theta \cos \theta & \tau' \cos^2 \theta & 0 \\ 0 & 0 & \tau - \tau' \end{bmatrix} \quad (3a)$$

Tension:

$$\mathbf{T}^{\text{tot}} = \begin{bmatrix} \tau' \sin^2 \theta & \tau' \sin \theta \cos \theta & 0 \\ \tau' \sin \theta \cos \theta & \tau + \tau' \cos^2 \theta & 0 \\ 0 & 0 & -\tau - \tau' \end{bmatrix} \quad (3b)$$

Strike-slip:

$$\mathbf{T}^{\text{tot}} = \begin{bmatrix} -\tau + \tau' \sin^2 \theta & \tau' \sin \theta \cos \theta & 0 \\ \tau' \sin \theta \cos \theta & \tau + \tau' \cos^2 \theta & 0 \\ 0 & 0 & \tau \end{bmatrix} \quad (3c)$$

The principal directions of this summed tensor will in most cases differ by rotation about a vertical axis from the principal directions of both  $\mathbf{T}$  and  $\mathbf{T}'$ . The  $x''$ - $y''$ - $z$  reference frame is defined to coincide with the principal axes of  $\mathbf{T}^{\text{tot}}$  so that the  $x''$  axis corresponds to the direction of maximum horizontal compressional stress. The angle  $\theta'$  is defined as the angle between the directions of the  $x$  axis and the  $x''$  axis (Figure 1). Thus  $\theta'$  is the angle by which the presence of a linear density anomaly causes the directions of the horizontal principal stresses of the summed stress tensor  $\mathbf{T}^{\text{tot}}$  to differ from the principal stress directions of the reference state (when there is no density anomaly).

The orientation of the principal axes of  $\mathbf{T}^{\text{tot}}$  are found in the usual manner, that is, by transforming  $\mathbf{T}'$  into the  $x''$ - $y''$ - $z$  reference frame by rotating it through the angle  $\theta'$ , setting the off-diagonal components to zero, and solving for  $\theta'$ . For the case of Equation (1c), when the reference state is strike-slip, the principal axes are at angles of

$$\frac{1}{2} \tan^{-1} \left[ \frac{\sin 2\theta}{-2\tau / \tau' - \cos 2\theta} \right] \quad (4)$$

$$\frac{1}{2} \tan^{-1} \left[ \frac{\sin 2\theta}{-2\tau / \tau' - \cos 2\theta} \right] + \frac{\pi}{2}$$

relative to the  $x$  axis.

When  $\mathbf{T}$  represents either a compressional or extensional state of stress, these angles are

$$\frac{1}{2} \tan^{-1} \left[ \frac{\sin 2\theta}{-\tau / \tau' - \cos 2\theta} \right]$$

$$\frac{1}{2} \tan^{-1} \left[ \frac{\sin 2\theta}{-\tau / \tau' - \cos 2\theta} \right] + \frac{\pi}{2} \quad (5)$$

The two solutions (Equations (4) and (5)) differ only by the factor of two in front of the term  $\tau / \tau'$ .

### 3. GENERAL RESULTS

#### 3.1. Change in Orientation of Horizontal Principal Stresses

The angular amount  $\theta'$  by which the orientation of the horizontal principal stresses changes in the presence of buoyancy forces depends simply on two factors. One is the ratio of the magnitude of the regional stresses and the

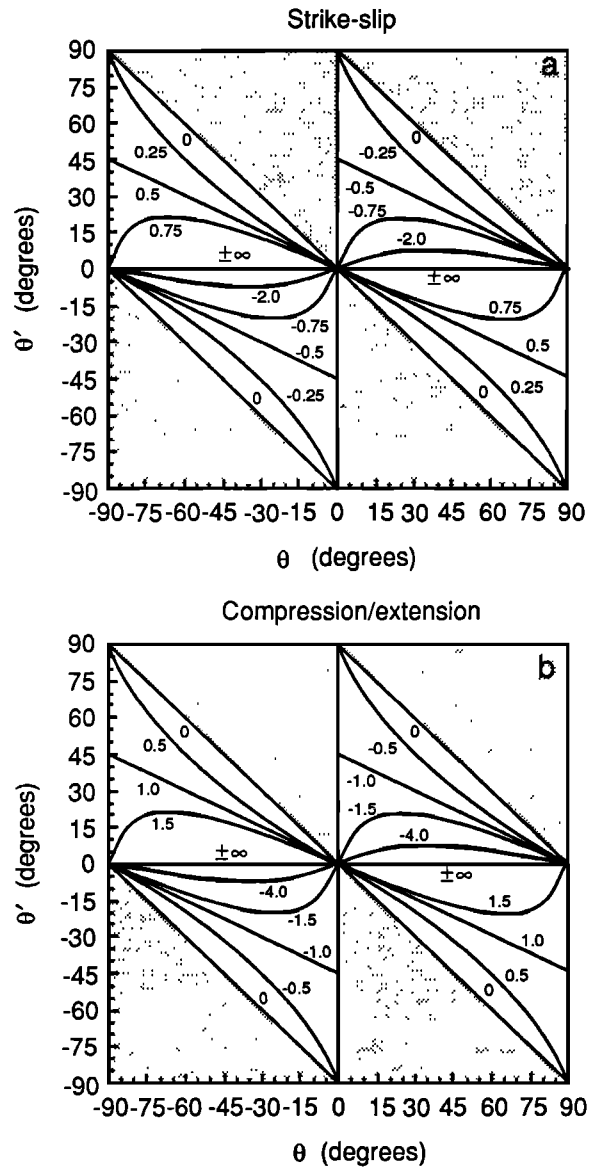


Fig. 2. Change in orientation ( $\theta'$ ) of principal horizontal compressive stress as a function of  $\theta$ . Numbers on curves refer to values of  $\tau/\tau'$ . Stippling indicates fields that are physically inaccessible. (a) Strike-slip reference state ( $\mathbf{T}$ ). (b) Compressional and extensional reference states ( $\mathbf{T}$ ).

magnitude of the stress arising from the density anomaly, expressed as  $\tau/\tau'$ . The other factor,  $\theta$ , characterizes the geometry of the system. Figure 2 shows how  $\theta'$  depends on these two parameters. Consider first the curve with  $\tau/\tau' = \pm \infty$ . In this case the buoyancy forces due to the density anomaly are negligible, so that  $T^{\text{tot}}$  is identical to  $T$  and  $\theta'$  is zero.

Conversely, as  $\tau/\tau' \rightarrow 0$ , stresses due to the buoyancy forces dominate, so that the principal horizontal stresses of  $T^{\text{tot}}$  become parallel to the  $x'$  and  $y'$  axes (see Figure 1). The sign of  $\tau'$  determines the axis to which  $x''$  is parallel. When  $\tau'$  is negative, the principal stress normal to the trend of the density anomaly is compressive, so that  $x''$  is parallel to the  $y'$  axis and  $\theta'$  differs from  $\theta$  by  $90^\circ$ . When  $\tau'$  is positive, the greatest horizontal compressive stress direction is parallel to the trend of the density anomaly, so  $\theta' = -\theta$ .

For intermediate values of  $\tau/\tau'$  the orientation of the principal axes of  $T^{\text{tot}}$  generally differs from that of both  $T$  and  $T'$ . In general, the effect of a negative density anomaly ( $\tau' < 0$ ) is to rotate the principal horizontal compressive stress direction toward the normal to the trend of the density anomaly, and that of a positive density anomaly ( $\tau' > 0$ ) is to rotate the principal horizontal compressive stress direction away from the normal.

Discontinuities in the curves (for example, for the strike-slip case, when  $\tau/\tau' = +0.5$  and  $\theta = \pm 90^\circ$  or when  $\tau/\tau' = -0.5$  and  $\theta = 0$ ) occur when the two horizontal principal stresses of  $T^{\text{tot}}$  become equal, so that neither can be uniquely identified as the greatest or least principal horizontal compressive stress.

### 3.2. Style of Deformation

The style of deformation, as well as the orientation of the horizontal stresses, can change as the result of the superposition of the stress due to buoyancy forces and the reference stress. According to Anderson's [1951] faulting criteria, the relative magnitudes of the principal stresses determine the faulting regime: depending on whether the vertical stress is the greatest, intermediate, or least principal stress, normal, strike-slip, or thrust faulting, respectively, is predicted. Figure 3 shows predicted faulting regimes based on Anderson's criteria and provides useful insight into how variations in buoyancy forces can affect the tectonic setting of a region. For each reference state and orientation of the density anomaly, each one of the three faulting regimes is possible in some range of  $\tau$  and  $\tau'$ . When the absolute value of  $\tau/\tau'$  is large, the influence of the density anomaly is small, so that the predicted faulting style remains the same as that of the reference state. On the other hand, when  $\tau/\tau'$  is small, the density anomaly has a large effect, so the sign of  $\tau/\tau'$  determines the faulting style. Thus, when  $\tau/\tau'$  is small and negative, the vertical stress is always the least compressive, so thrust faulting is expected; when  $\tau/\tau'$  is small and positive, the vertical stress is always the most compressive stress, hence normal faulting is predicted.

For intermediate values of  $\tau/\tau'$ , the type of faulting depends on the relative orientation of the reference stress state and the trend of the density anomaly. Small changes in the relative magnitudes of  $\tau$  and  $\tau'$  can change the style of deformation between strike-slip and normal faulting, or strike-slip and

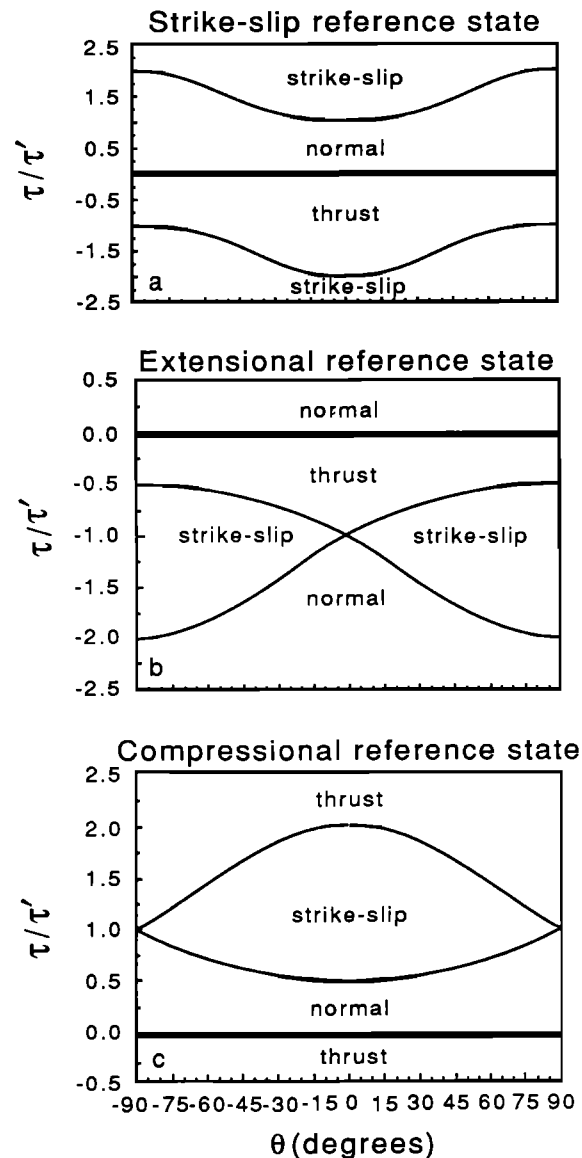


Fig. 3. Expected faulting style, according to Anderson's [1951] theory, as a function of  $\tau/\tau'$  and  $\theta$ . Note that no failure criterion was considered, so plots indicate the faulting regime assuming that failure has occurred. (a) Strike-slip reference state. (b) Extensional reference state. (c) Compressional reference state.

thrust faulting [cf. Dalmayrac and Molnar, 1981; Froidevaux and Isacks, 1984; Molnar and Lyon-Caen, 1988]. Alternatively, if the relative magnitudes of the stresses remain constant, but  $\theta$  changes over time (for example, by a change in the orientation of the regional stress field or by finite deformation that results in a rotation of the density anomaly) then the style of subsequent deformation can be greatly changed.

In considering Figure 3, it is important to note that whether or not faulting with the indicated style occurs will depend on the magnitudes of the stresses in relation to the failure strength of the crust. If the upper crust is strong and deforms by slip according to Byerlee's Law, then large changes in the magnitudes of the greatest and least principal stresses are needed to move across the boundary between the normal faulting and thrust faulting fields. This is represented in Figure 3 by heavy lines between these fields. However, for transitions between strike-slip and normal faulting, or strike-slip and thrust faulting, the changes in magnitude of stress components can be small.

#### 4. COMPARISON OF THE MODEL TO THE TRANSVERSE RANGES, CALIFORNIA

##### 4.1. Tectonics of the Transverse Ranges

Most geological and physiographical features of California south of the Mendocino triple junction trend northwesterly and can be related to regional northwest-southeast shearing associated with relative motions of the Pacific and North American plates. An obvious exception is the Transverse Ranges province, which trends east-west across the strike of most other structures (Figure 4a). The province also differs

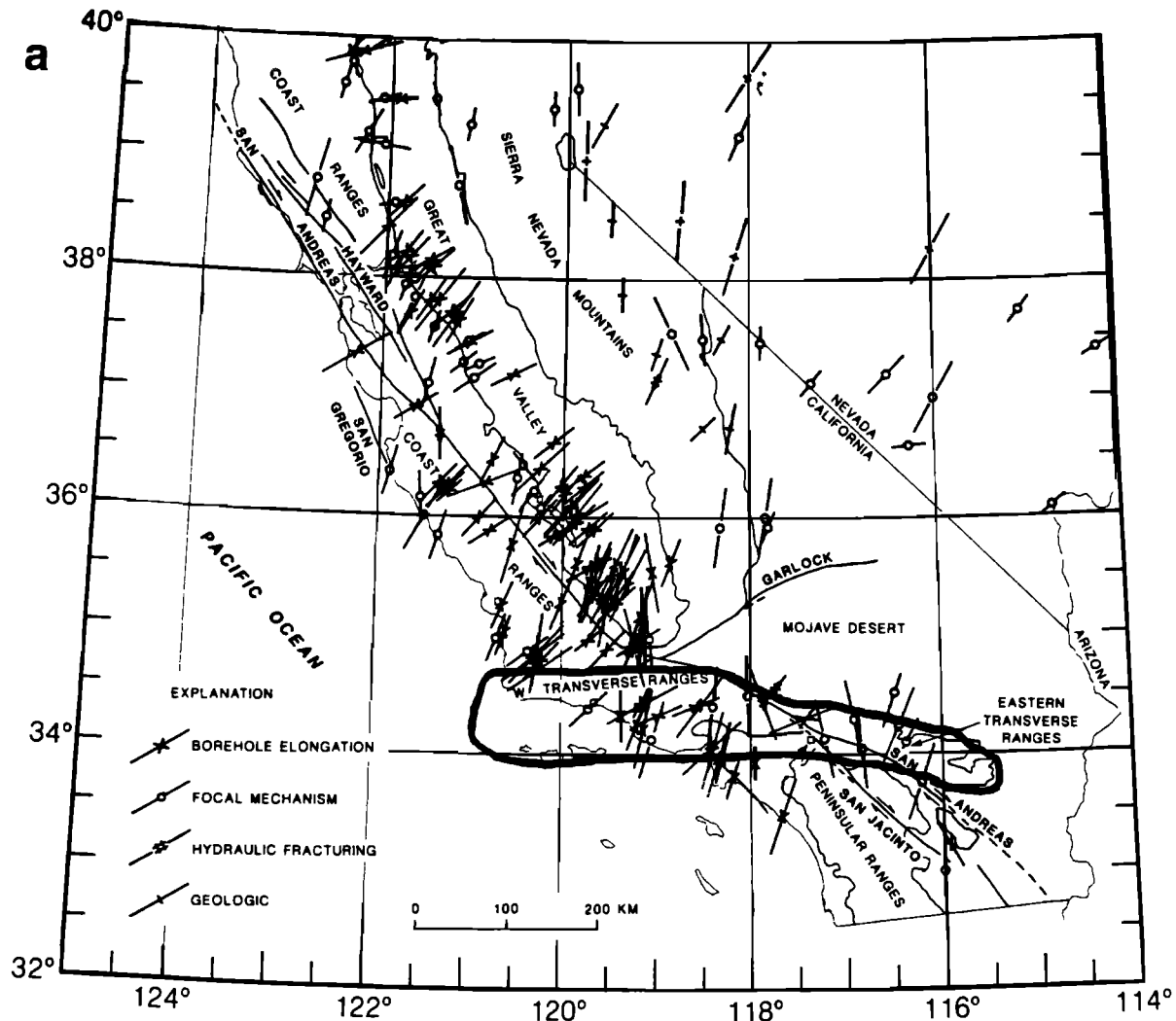


Fig. 4. (a) Principal stress direction data in California. Short lines indicate the orientation of the maximum horizontal compressive stress. Heavy line outlines Transverse Ranges Province. Adapted from Zoback et al. [1987]. (b) Rose diagrams showing principal horizontal compressive stress directions and mean azimuths (squares). Radii of circles represent 20% of the data; N is the size of each data set. Diagram for central California includes data located north of latitude 35.5° N and west of the Sierra Nevada physiographic province (see Figure 4a). Data used in the Transverse Ranges plot are located between latitudes 33.5° N and 34.5° N and west of longitude 115.5° W. Data are from Figure 4a and M. D. Zoback (private communication, 1989).

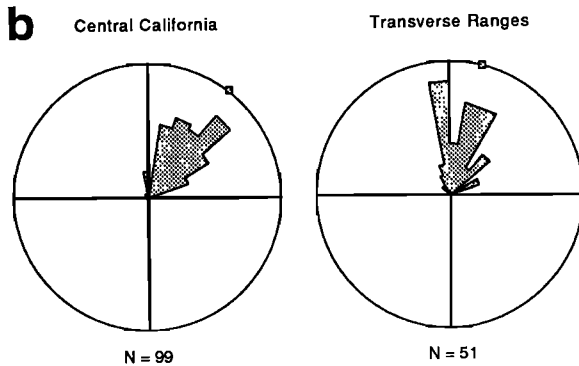


Fig. 4 (continued)

from other locations along the San Andreas fault in that east-west trending thrust faults and folds with east-west axes are observed, in contrast to the northwest-trending faults and fold axes found in the central California Coast Ranges and in areas south of the Transverse Ranges.

The San Andreas fault, which presently accommodates about two-thirds of the Pacific-North America relative plate motion of 5 to 6 cm yr<sup>-1</sup> [DeMets et al., 1986; Minster and Jordan, 1984, 1987], trends about N 35° W in central California, but where it cuts through the Transverse Ranges it trends more westerly by about 20° to 30°, resulting in the "big bend" (Figure 4a). The most widely accepted hypothesis for the origin of the late Cenozoic uplift of the Transverse Ranges is that movement along the right-lateral San Andreas fault caused compression and horizontal shortening along the length of the left-stepping "big bend" in the fault (e.g., Crowell [1979] and many others). However, this explanation is not entirely satisfactory because it requires the "big bend" to exist prior to the compression and hence does not address the problem of how or why the "big bend" originated. The model presented in this paper, when applied to the tectonics of the Transverse Ranges, provides not only insight into the possible origins of the variations in orientation of principal stresses in California, but an alternative explanation for the origin of the "big bend".

To compare the predictions of the model to the tectonics of the Transverse Ranges, I use structural and geophysical observations to constrain  $\theta$  and  $\theta'$ , and use these to estimate the range of  $\tau/\tau'$  appropriate to the Transverse Ranges. The model is tested by comparing the predicted values of  $\tau/\tau'$  with independently derived estimates of  $\tau$  and  $\tau'$ .

#### 4.2. Observations of Stress Orientations in California

Zoback et al. [1987] summarized most of the available stress direction data for California, including borehole data, young (< 2 Ma) volcanic alignments, and earthquake focal mechanisms. Figure 4a, from Zoback et al. [1987], suggests that principal horizontal compressive stress directions are northeast-southwest in central California and the region south of the Transverse Ranges, but in the Transverse Ranges province the maximum compressive stress directions are oriented more northerly. Also note that, as the trend of the San Andreas fault changes as it passes through the Transverse Ranges, the maximum compressional stress directions remain

approximately perpendicular to it. Figure 4b shows rose diagrams for two data subsets of Zoback et al. [1987, also M. D. Zoback, private communication, 1989]. The mean directions for central California and the Transverse Ranges, listed in Table 1, are statistically distinct from each other. In addition, within the uncertainties, the mean direction determined for central California is statistically indistinct from that of N 43.9° ± 1.9° determined by Mount and Suppe [1987] from a different subset of the Zoback et al. [1987] data compilation.

TABLE 1. Mean Principal Horizontal Compressive Stress Directions

Region	N <sup>a</sup>	Mean Azimuth <sup>b</sup>	Radius of 95% Confidence Interval <sup>b</sup> (deg)
Central California	99	N 37 E	8
Transverse Ranges	51	N 14 E	12

<sup>a</sup>Number of observations.

<sup>b</sup>Determined using methods from Mardia [1972].

In terms of the model for stress rotation presented earlier (sections 2 and 3 and Figure 1), these data allow estimates to be made of  $\theta$  and  $\theta'$ . The average direction of the maximum horizontal compressive stress in central California is N 37° E (Table 1) and the trend of the density anomaly under the Transverse Ranges is about N 90° E [Humphreys et al., 1984], so  $\theta$  should be approximately 53°. In the Transverse Ranges the mean direction of the maximum horizontal compressional stress is N 14° E, so  $\theta'$  is approximately 23°. The 95% confidence intervals listed in Table 1 provide some measure of uncertainty in  $\theta$  and  $\theta'$ . If the trend of the Transverse Ranges anomaly is assumed to be uncertain by ±10°, then the range of  $\theta$  is between 35° and 71°; the permissible range of  $\theta'$  is between 3° and 43°. These ranges are plotted in Figure 5a and show that the range of  $\tau/\tau'$  is constrained to be between 0 and -4, with a value of -0.4 most probable, corresponding to the mean values of  $\theta$  and  $\theta'$ .

It is not the purpose of this paper to offer an explanation for the observation that maximum horizontal compressive stresses are perpendicular to the San Andreas fault; Zoback et al. [1987] and Mount and Suppe [1987] have proposed that this may be attributed to the mechanical weakness of the San Andreas fault. Instead, I concentrate on the observation that both the stresses and the San Andreas fault differ in orientation within the Transverse Ranges, compared with their orientations in central California. I show below that the model presented above can account for the orientation of the stresses in the Transverse Ranges; in addition, if, for whatever reason, within the Transverse Ranges the San Andreas fault maintains the same angle with respect to the stresses as it does in central California, the model also offers some insight into the cause of the "big bend" in the San Andreas fault.

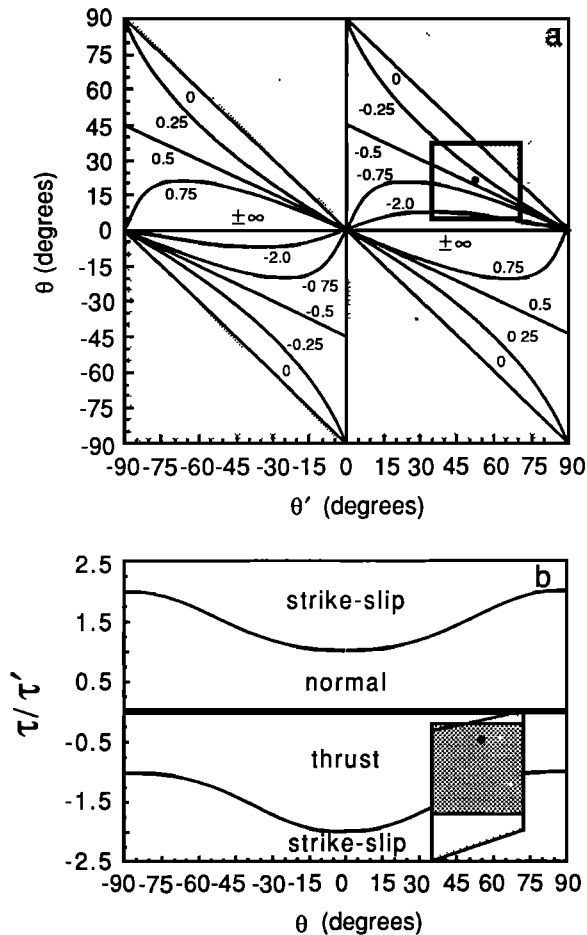


Fig. 5. (a) As Figure 2a. Box indicates range of  $\theta$  and  $\theta'$  determined from observations in California. (b) As Figure 3a. Boxes indicate the ranges determined from constraints on  $\theta$  and  $\theta'$  (light stippling) as described in text, and from observational constraints on  $\tau$  and  $L$  (dark stippling). Dots show values obtained from the mean principal stress directions.

#### 4.3. Independent estimate of $\tau$

The lack of a localized heat flow anomaly associated with the San Andreas fault has been used to constrain the frictional shear stress on the San Andreas fault to be less than 20 MPa [Lachenbruch and Sass, 1980; 1981].

Both lower and upper bounds for  $\tau$  can be estimated using a slightly different reasoning [Sonder and England, 1986]. A region in central California, 75-100 km wide and centered over the Coast Ranges, has a mean heat flux that is 20-40 mW m<sup>2</sup> greater than that found to the east [e.g., Lachenbruch and Sass, 1980, Figure 15]. If this anomaly results entirely from shear dissipation within the lithosphere then  $\tau$  must be between 8 and 18 MPa for ambient shear strain rates around 9-10 x 10<sup>-15</sup> s<sup>-1</sup> [Savage et al., 1981; Thatcher, 1975, 1983] and a lithosphere thickness of 120 km.

#### 4.4. Evidence for a Density Anomaly Under the Transverse Ranges and Independent Estimate of $\tau'$

Several analyses of earthquake travel-time data have shown that arrival times for P waves travelling through the Transverse Ranges province are 0.5 to 1 second early compared with those for waves with paths outside the Transverse Ranges [Hadley and Kanamori, 1977; Raikes, 1980; Walck and Minster, 1982], suggesting the presence of higher densities underneath the Transverse Ranges. This has been confirmed by a seismic tomography study by Humphreys et al. [1984] that reveals a vertical, wedge-shaped region extending to a depth of 100 to 250 km which is 2-3% faster than its surroundings. The region correlates well with the location of the Transverse Ranges and is approximately 300 km (E-W) by 100 km (N-S) in horizontal extent. If this high velocity region is interpreted as being the result of cold temperatures, it follows that there should be a significant density anomaly under the Transverse Ranges. Using values for  $dVp/dT$  of  $-0.5 \text{ m s}^{-1} \text{ deg}^{-1}$  and  $\partial\rho/\partial T$  of  $-0.11 \text{ kg m}^{-3} \text{ deg}^{-1}$  (at 1250 °C) from Anderson and Bass [1984], where  $Vp$  is P wave velocity,  $T$  is temperature, and  $\rho$  is density, gives a value for  $dVp/d\rho$  of  $4.4 \text{ m}^4 \text{ s}^{-1} \text{ kg}^{-1}$ . Combined with the observed velocity anomaly of 2-3% under the Transverse Ranges [Humphreys et al., 1984], this suggests a density anomaly of approximately 40 - 60 kg m<sup>-3</sup>, or 1 - 2%.

Taking the top of the density anomaly at the Moho (30 km depth), if it extends to 250 km, then  $L = 220 \text{ km}$ , so the magnitude of the mass anomaly  $\Delta\rho L$  is around  $0.9 - 1.5 \times 10^7 \text{ kg m}^{-2}$ , for the range of  $\Delta\rho$  determined above. If the density anomaly extends only to 150 km depth, as in the western Transverse Ranges, the mass anomaly is less, between  $4.8$  and  $8.4 \times 10^6 \text{ kg m}^{-2}$ . Figure A2 shows that, for the half-width of the density anomaly (about 50 km) equal to its depth, the surface magnitude of the deviatoric stresses is approximately  $\Delta\rho g L/3$ . Therefore,  $\tau'$  can be as large as 49 MPa, if  $L = 220 \text{ km}$  and  $\Delta\rho = 70 \text{ kg m}^{-3}$ , or as small as 16 MPa, if  $L = 120 \text{ km}$  and  $\Delta\rho = 40 \text{ kg m}^{-3}$ .

Taking these constraints on  $\tau$  and  $\tau'$  gives a range of  $\tau/\tau'$  between  $-0.16$  and  $-1.1$ , which includes the mean value of  $-0.4$  predicted earlier and matches well with the field that was obtained using the observational limits on  $\theta$  and  $\theta'$  (see Figure 5a). The agreement suggests that the simple model presented here can account for the observed variation in principal stress directions between the Transverse Ranges and other parts of the Pacific-North America plate boundary zone in California.

## 5. DISCUSSION

Several different hypotheses have been proposed for the origin of the velocity anomaly underneath the Transverse Ranges. Sheffels and McNutt [1986] suggested that it was the result of intracontinental subduction due to compression across the Transverse Ranges. However, if the downdip length of the velocity anomaly is taken as indicative of the amount of convergence, then there must have been as much as 200 km of convergence across the central Transverse Ranges. Weldon and Humphreys [1986] point out that the volume of crust involved in this amount of convergence far exceeds the present-day

volume of crust in the Transverse Ranges. In addition, the intracontinental subduction hypothesis does not explain why or when compression developed across the Transverse Ranges in the first place.

Humphreys et al. [1984] propose that the seismically fast region under the Transverse Ranges is a negatively buoyant convective instability. Such a feature does not require pre-existing compression to develop; the time-dependent and chaotic nature of convection in the earth's mantle permits the development of convective instabilities anywhere along the base of the thermal boundary layer. If the hypothesis that the density anomaly is a convective instability is tentatively adopted, then a speculative but highly intriguing consequence arises. The instability may have been smaller in the past, and, if  $\tau$  has remained relatively constant,  $\tau/\tau'$  would have been more negative in earlier times. Figure 5 shows that the present-day means of  $\theta$  and  $\tau/\tau'$  plot in the field where thrusting is expected to dominate. However, if  $\tau/\tau'$  was more negative, the mean values of  $\theta$  and  $\tau/\tau'$  would be more likely to plot in the strike-slip field. Thus the growth of a convective instability provides a mechanism by which the style of deformation in the Transverse Ranges may have changed from dominantly strike-slip to dominantly thrusting. Support for this speculation may be provided by evidence in the San Bernardino mountains that earliest deformation on thrust faults occurred between 9.5 and 4.1 Ma, at a time when strike-slip deformation was already active on the San Gabriel fault; compressional deformation may have begun even later in the San Gabriel mountains [Meisling and Weldon, 1989].

This simple model for the orientation of principal stresses has an important implication for the relationship between the deformation producing the Transverse Ranges and the "big bend" of the San Andreas fault. Rather than the Transverse Ranges being formed by compression across a spatially fixed "big bend", as has been commonly assumed, both the Transverse Ranges and the "big bend" can be understood to be consequences of the negative buoyancy force under the Transverse Ranges. If the San Andreas fault maintains the same high angle to the maximum horizontal compressional stress as it does in central California [Mount and Suppe, 1987; Zoback et al., 1987], then progressive counterclockwise change in direction of the maximum horizontal compressive stress would imply a corresponding counterclockwise rotation of the trend of the San Andreas fault, thus producing a bend in the fault as it passes through the Transverse Ranges.

## 6. CONCLUSIONS

I have used a simple model to investigate the effect of a density anomaly on an otherwise regionally constant stress field, and have emphasized changes in the orientation and relative magnitudes of the principal stresses. If the density of the anomaly exceeds that of its surroundings (that is, produces a negative buoyancy force), the effect on the state of stress within the lithosphere is to increase the angle between the maximum horizontal compressional stress direction and the trend of the linear density anomaly. The angle decreases if the buoyancy forces are positive (density of the anomaly is less than its surroundings). The relative magnitudes of the principal stresses can also be affected, potentially altering the expected

style of deformation for example, in the instance of the California Transverse Ranges, from dominantly strike-slip to dominantly thrusting). The sense and magnitude of these changes depend on two parameters: first, the relative magnitudes of the regional deviatoric stress and the deviatoric stress due to the local buoyancy forces, and second, the trend of the density anomaly in relation to the direction of the principal horizontal compressive stress of the regional, unperturbed, stress tensor.

The principal horizontal stresses in the Transverse Ranges are oriented northerly, in contrast to the northeasterly directions observed in central California and California south of the Transverse Ranges. Also, there is good seismological evidence for a wedge-shaped region of high density underneath the Transverse Ranges. From the trend of the density anomaly and the 23° difference in orientation of principal stress directions within and outside the Transverse Ranges, the ratio of the magnitudes of the regional stress associated with strike-slip deformation and the local stress due to the density anomaly is predicted to be approximately -0.4, with a range of 0 to -4. This range is consistent with that estimated independently from consideration of the differences in seismic velocity under the Transverse Ranges and their surroundings, and the lack of a large heat flow anomaly associated with deformation along the San Andreas fault in central California. Hence, the model presented here, although certainly not the only possible explanation of the stress orientation data, does provide a simple understanding of the observed variations in stress state along the San Andreas fault in California. The success of the model when applied to California supports the speculation that both the uplift and compression in the Transverse Ranges and the formation of the "big bend" of the San Andreas fault are attributable to the same cause, namely the formation and growth of a convective downwelling under the Transverse Ranges [Humphreys et al., 1984].

## APPENDIX A: STRESSES RESULTING FROM A BURIED DENSITY ANOMALY

The density anomaly is assumed to have constant magnitude  $\Delta\rho$ , and to extend over a width  $2w$  in the  $y'$  direction and over a depth range  $L$  (Figure A1a). Its length in the  $x'$  direction is assumed to be much greater than its dimensions in either the  $y'$ -direction or  $z$  direction, so that variations of density in the  $x'$ -direction can be neglected and the equations of motion are reduced to their two-dimensional form. In addition, in order to simplify the solution of the equations of motion, the density anomaly is approximated by expressing it as a constant mass anomaly  $\Delta m = \Delta\rho L$ , collapsed onto the surface  $z = d$ , with width  $2w$  in the  $y'$  direction (Figure A1b). This allows the solution domain to be divided into two regions, an upper layer and a lower half-space, both of uniform density and viscosity, separated by the anomalous surface mass distribution at  $z = d$ .

A Fourier series solution to the equations of motion is described below; thus the anomalous mass distribution  $\Delta m$  must be made periodic. Figure A1c shows this periodic extension of the mass distribution; the wavelength  $2\lambda$  is taken to be much greater than the width  $2w$  of the mass anomaly, so that the stress distribution in the region  $|y'| \leq w$  approximates that of a single, isolated mass anomaly. For an anomaly  $\Delta m$

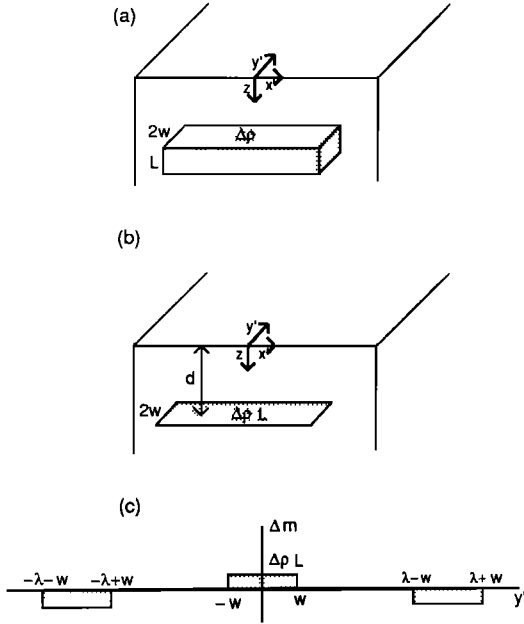


Fig. A1. (a) Coordinate system and parameters used to describe a region of anomalous density  $\Delta\rho$ , width  $2w$ , and thickness  $L$ . (b) Density anomaly is collapsed onto the horizontal surface  $z = d$ ; the mass anomaly per unit area is  $\Delta\rho L$ . (c) Periodic extension of the mass anomaly. Width is  $2w$ , wavelength  $2\lambda$ , magnitude  $\pm\Delta\rho L$ .

of constant magnitude  $\Delta\rho L$ , with width  $2w$  and wavelength  $2\lambda$ , the Fourier series and coefficients  $\delta m$  are given by:

$$\Delta m = \sum_{n=1}^{\infty} \delta m_n \cos(n\pi y'/\lambda) \quad (\text{A1})$$

$$\delta m_n = \begin{cases} \frac{4 \Delta\rho L}{n\pi} \sin\left(\frac{n\pi w}{\lambda}\right) & n \text{ odd} \\ 0 & n \text{ even} \end{cases}$$

For each term in the Fourier series, the stress distribution is found, following the method described by, among many others, Fleitout and Froidevaux [1982, Appendix A1]. The total stress field is found by superposition of each Fourier component.

In the absence of inertial forces, the equations of motion for a uniform incompressible Newtonian viscous fluid can be written

$$\frac{\partial^2 v}{\partial y'^2} + \frac{\partial^2 v}{\partial z^2} = \frac{1}{\eta} \frac{\partial p}{\partial y'} \quad (\text{A2})$$

$$\frac{\partial^2 w}{\partial y'^2} + \frac{\partial^2 w}{\partial z^2} = \frac{1}{\eta} \frac{\partial p}{\partial z}$$

where  $v$  and  $w$  are the  $y'$  and  $z$  components of velocity,  $p$  is the nonhydrostatic pressure, and  $\eta$  is viscosity. Within each

layer (see Figure A1) the general solution to (A2) is

$$v = \sin\left(\frac{n\pi y'}{\lambda}\right) \left[ -\left(A + B + B \frac{n\pi z}{\lambda}\right) e^{n\pi z/\lambda} + \left(C - D + D \frac{n\pi z}{\lambda}\right) e^{-n\pi z/\lambda} \right] \quad (\text{A3})$$

$$w = \cos\left(\frac{n\pi y'}{\lambda}\right) \left[ \left(A + B \frac{n\pi z}{\lambda}\right) e^{n\pi z/\lambda} + \left(C + D \frac{n\pi z}{\lambda}\right) e^{-n\pi z/\lambda} \right]$$

where  $A$ ,  $B$ ,  $C$ , and  $D$  are constants of integration.

Boundary conditions on  $z = 0$  are zero shear stress ( $\tau_{y'z} = 0$ ) and zero vertical velocity ( $w = 0$ ). Velocities are bounded as  $z \rightarrow \infty$ . At the interface  $z = d$  between the layers, velocities and shear stress are continuous and there is a step change  $g\delta m$  in vertical stress, due to the mass anomaly. For these boundary conditions,

$$A_1 = \frac{-\delta m g \lambda}{4\eta n \pi} \left(-1 - \frac{n\pi d}{\lambda}\right) e^{-n\pi d/\lambda}$$

$$B_1 = \frac{-\delta m g \lambda}{4\eta n \pi} e^{-n\pi d/\lambda}$$

$$C_1 = \frac{-\delta m g \lambda}{4\eta n \pi} \left(1 + \frac{n\pi d}{\lambda}\right) e^{-n\pi d/\lambda}$$

$$D_1 = \frac{-\delta m g \lambda}{4\eta n \pi} e^{-n\pi d/\lambda}$$

$$A_2 = 0$$

$$B_2 = 0$$

$$C_2 = \frac{-\delta m g \lambda}{4\eta n \pi} \left[ \left(-1 + \frac{n\pi d}{\lambda}\right) e^{n\pi d/\lambda} + \left(1 + \frac{n\pi d}{\lambda}\right) e^{-n\pi d/\lambda} \right]$$

$$D_2 = \frac{-\delta m g \lambda}{4\eta n \pi} \left(-e^{n\pi d/\lambda} + e^{-n\pi d/\lambda}\right) \quad (\text{A4})$$

where subscripts 1 and 2 refer to the upper layer and lower half space, respectively.

In the upper layer, the deviatoric stresses are

$$\tau_{y'y'} = g\Delta\rho L \sum_{n=1}^{\infty} [1 - (-1)^n] \cos\left(\frac{n\pi y'}{\lambda}\right) \sin\left(\frac{n\pi w}{\lambda}\right) e^{-n\pi d/\lambda} \cdot [e^{n\pi z/\lambda} (z-d)/\lambda - e^{-n\pi z/\lambda} (z+d)/\lambda]$$

$$\tau_{zz} = -g\Delta\rho L \sum_{n=1}^{\infty} [1 - (-1)^n] \cos\left(\frac{n\pi y'}{\lambda}\right) \sin\left(\frac{n\pi w}{\lambda}\right) e^{-n\pi d/\lambda} \cdot [e^{n\pi z/\lambda} (z-d)/\lambda - e^{-n\pi z/\lambda} (z+d)/\lambda] \quad (\text{A5})$$

$$\tau_{y'z} = g\Delta\rho L \sum_{n=1}^{\infty} [1 - (-1)^n] \sin\left(\frac{n\pi y'}{\lambda}\right) \sin\left(\frac{n\pi w}{\lambda}\right) e^{-n\pi d/\lambda} \cdot [e^{n\pi z/\lambda} (z-d)/\lambda + e^{-n\pi z/\lambda} (z+d)/\lambda]$$

At the surface the shear stress  $\tau_{y'z}$  is zero, and for  $z < w/2$ , the magnitude of the shear stress is always less than 10% of the magnitude of the normal stresses. Thus the near-surface deviatoric stress field is, to a good approximation, biaxial.

It remains to show how the magnitude of  $\tau_{zz}$  (or  $\tau_{y'y'}$ ) depends on the wavelength  $\lambda$  of the periodic extension of the mass anomaly, and how it varies with distance,  $y'$ , perpendicular to the trend of the anomaly. Figure A2 shows  $\tau_{zz}$  at  $z = 0$  as a function of horizontal distance  $y'$ . For  $\lambda > 5w$ ,  $\tau_{zz}$  does not depend strongly on  $\lambda/w$ . In the region above the center of the mass anomaly ( $|y'| < w/2$ ), the magnitude of the stress varies by less than 10% of its maximum value, so may be considered to be approximately constant. The stress is greatest above the center of the mass anomaly ( $y' = 0$ ) and decreases with horizontal distance. For  $|y'| > 4w/3$ , the stress is always less than 20% of its maximum value, so that the solution closely approximates that for a single isolated mass anomaly and is not strongly influenced by the periodic extensions of the mass anomaly that were introduced to obtain the Fourier series solution.

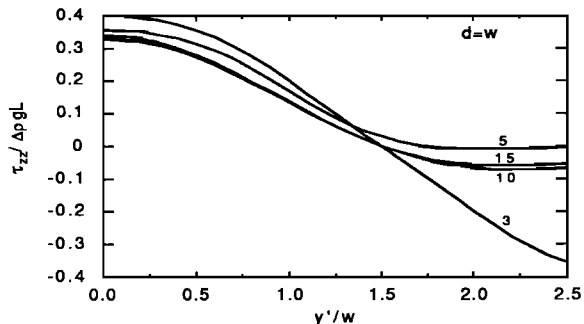


Fig. A2. Vertical deviatoric stress at  $z = 0$  as a function of  $y'/w$  for the mass anomaly distribution shown in Figure A1c. Numbers on curves refer to values of  $\lambda/w$ .

**Acknowledgments.** While part of this work was carried out I was supported by a Chaim Weizmann Postdoctoral Fellowship at Caltech. While I was there B. Hager generously provided funds for travel and miscellaneous costs (NASA grant NAG5-842). I thank P. England and E. Humphreys for helpful discussions, and C. Jones, S. King, M. D. Zoback, B. Sheffels, R. Westaway, and an anonymous reviewer for commenting on earlier versions of the manuscript. I am also grateful to M. D. Zoback for permission to use his figure and data compilation in this paper.

#### REFERENCES

Anderson, D. L., and J. D. Bass, Mineralogy and composition of the upper mantle, *Geophys. Res. Lett.*, **11**, 637-640, 1984.

- Anderson, E. M., *The Dynamics of Faulting*, Oliver and Boyd, Edinburgh, 1951.
- Artyushkov, E. V., Stresses in the lithosphere caused by crustal thickness inhomogeneities, *J. Geophys. Res.*, **78**, 7675-7708, 1973.
- Bott, M. H. P. and D. S. Dean, Stress systems at young continental margins, *Nature*, **235**, 23-25, 1972.
- Crowell, J. C., The San Andreas Fault system through time, *J. Geol. Soc. London*, **136**, 293-302, 1979.
- Dalmayrac, B., and P. Molnar, Parallel thrust and normal faulting in Peru and constraints on the state of stress, *Earth Planet. Sci. Lett.*, **55**, 473-481, 1981.
- DeMets, C., R. G. Gordon, S. Stein, D. Argus, and D. Woods, Pacific-North America spreading rate in the Gulf of California, *EOS Trans. AGU*, **67**, 905, 1986.
- Fleitout, L., and C. Froidevaux, Tectonics and topography for a lithosphere containing density heterogeneities, *Tectonics*, **1**, 21-56, 1982.
- Froidevaux, C., and B. L. Isacks, The mechanical state of the lithosphere in the Altiplano-Puna segment of the Andes, *Earth Planet. Sci. Lett.*, **71**, 305-314, 1984.
- Hadley, D., and H. Kanamori, Seismic structure of the Transverse Ranges, California, *Geol. Soc. Am. Bull.*, **88**, 1469-1478, 1977.
- Humphreys, E., R. W. Clayton, and B. H. Hager, A tomographic image of mantle structure beneath southern California, *Geophys. Res. Lett.*, **11**, 625-627, 1984.
- Lachenbruch, A. H., and J. H. Sass, Heat flow and energetics of the San Andreas fault zone, *J. Geophys. Res.*, **85**, 6185-6222, 1980.
- Lachenbruch, A. H., and J. H. Sass, Corrections to 'Heat flow and energetics of the San Andreas fault zone' and some additional comments on the relation between fault friction and observed heat flow, *J. Geophys. Res.*, **86**, 7171-7172, 1981.
- Mardia, K. V., *Statistics of Directional Data*, Academic, San Diego, Calif., 1972.
- Meisling, K. E., and R. J. Weldon, Late Cenozoic tectonics of the northwestern San Bernardino Mountains, southern California, *Geol. Soc. Am. Bull.*, **101**, 106-128, 1989.
- Minster, J. B., and T. H. Jordan, Vector constraints on Quaternary deformation of the western United States east and west of the San Andreas fault, in *Tectonics and Sedimentation along the California Margin*, edited by J. K. Crouch and S. B. Bachman, pp. 1-16, Soc. Econ. Paleontol. Mineral., Pac. Sect., 1984.
- Minster, J. B., and T. H. Jordan, Vector constraints on western U.S. deformation from space geodesy, neotectonics, and plate motions, *J. Geophys. Res.*, **92**, 4798-4804, 1987.
- Molnar, P., and H. Lyon-Caen, Some simple physical aspects of the support, structure, and evolution of mountain belts, *Spec. Pap. Geol. Soc. Am.*, **218**, 179-207, 1988.
- Mount, V. S., and J. Suppe, State of stress near the San Andreas fault: implications for wrench tectonics, *Geology*, **15**, 1143-1146, 1987.
- Raikes, S. A., Regional variations in upper mantle structure beneath southern California, *Geophys. J. R. Astron. Soc.*, **63**, 187-216, 1980.
- Savage, J. C., W. H. Prescott, M. Lisowski, and N. E. King, Strain accumulation in southern California, *J. Geophys. Res.*, **86**, 6991-7001, 1981.
- Sheffels, B., and M. McNutt, Role of subsurface loads and regional compensation in the isostatic balance of the Transverse Ranges, California: Evidence for intracontinental subduction, *J. Geophys. Res.*, **91**, 6419-6431, 1986.

- Sonder, L. J., and P. C. England, Vertical averages of rheology of the continental lithosphere: Relation to thin sheet parameters, *Earth Planet. Sci. Lett.*, 77, 81-90, 1986.
- Thatcher, W., Strain accumulation on the northern San Andreas fault since 1906, *J. Geophys. Res.*, 80, 4873-4880, 1975.
- Thatcher, W., Nonlinear strain buildup and the earthquake cycle on the San Andreas fault, *J. Geophys. Res.*, 88, 5893-5902, 1983.
- Walck, M. C., and J. B. Minster, Relative array analysis of upper mantle velocity variations in southern California, *J. Geophys. Res.*, 87, 1757-1772, 1982.
- Weldon, R., and E. Humphreys, A kinematic model of southern California, *Tectonics*, 5, 33-48, 1986.
- Zoback, M. D., M. L. Zoback, V. S. Mount, J. Suppe, J. P. Eaton, J. H. Healy, D. Oppenheimer, P. Reasenber, L. Jones, C. B. Raleigh, I. G. Wong, O. Scotti, and C. Wentworth, New evidence on the state of stress of the San Andreas fault system, *Science*, 238, 1105-1111, 1987.

---

L. Sonder, Department of Earth Sciences, Fairchild Science Center, Dartmouth College, Hanover, NH 03755.

(Received October 11, 1989;  
revised January 29, 1990;  
accepted February 2, 1990.)